Archives of Advances in Biosciences

Original Article

OPEN ACCESS

Suppression of CircPVT1 Potentiates 5-Fluorouracil-Driven Programmed Cell Death in SK-MEL-37 Malignant Melanoma Cells: Role of the miR-203a-3p/FGF2 Regulatory Cascade

Zahra Yousefian Naeini[1], Mehrdad Hashemi[2,3*], Masoumeh Heshmati[1], Ali Jebali[4], Maliheh Entezari[2,3]

[1.] Department of Cellular and Molecular Biology, TeMS.C., Islamic Azad University, Tehran, Iran.
[2.] Department of Genetics, TeMS.C., Islamic Azad University, Tehran, Iran.
[3.] Farhikhtegan Medical Convergence Sciences Research Center, Farhikhtegan Hospital, Faculty of medicine,TeMS.C., Islamic Azad University, Tehran, Iran. Email: mhashemi@iau.ac.ir
[4.] Department of Nanobiotechnology, TeMS.C., Islamic Azad University, Tehran, Iran.

Received: 14 Jun 2026; **Accepted:** 05 Aug 2026; **Published:** 06 Oct 2026

Cite this article as: Yousefian Naeini Z, Hashemi M, Heshmati M, Jebali A, Entezari M. Suppression of CircPVT1 Potentiates 5-Fluorouracil-Driven Programmed Cell Death in SK-MEL-37 Malignant Melanoma Cells: Role of the miR-203a-3p/FGF2 Regulatory Cascade. Archives of Advances in Biosciences. 2026 17(1):1-13. https://doi.org/10.22037/aab.v17i1.52479

Abstract

Background and Aim: The circular RNA, known as CircPVT1, functions as an oncogenic molecule across several.
Methods: SK-MEL-37 cultures were assigned to five experimental conditions: untreated controls, non-targeting scrambled siRNA (40 nM), CircPVT1-directed siRNA (40 nM), 5-FU alone (500 µM), and the siRNA/5-FU combination. Transfection employed TurboFect reagent. Following a 48-hour exposure, viability was evaluated through MTT colorimetry. Apoptotic rates were determined via Annexin V-FITC/propidium iodide dual labeling coupled with flow cytometry. Quantitative real-time PCR measured transcript levels of CircPVT1, miR-203a-3p, FGF2, Bax, Bcl-2, and Caspase-3. Bioinformatic tools (circInteractome, TargetScan, miRDB) predicted possible interactions within the CircPVT1/miR-203a-3p/FGF2 network.
Results: In silico analysis revealed a potential miR-203a-3p docking site inside CircPVT1 and identified FGF2 as a genuine miR-203a-3p target carrying a conserved 3′UTR recognition sequence. MTT data showed that anti-CircPVT1 siRNA lowered viability to 48.3% of control values, whereas 5-FU alone dropped viability to 44.2%. The combined regimen produced the strongest reduction, yielding 28.6% viability ($p<0.001$ versus controls; $p<0.01$ versus each monotherapy). Flow cytometry indicated that the combination elevated late-stage apoptosis to 24.3%, compared with 17.9% for siRNA alone and 15.7% for 5-FU alone ($p<0.001$). qRT-PCR revealed that the combination upregulated miR-203a-3p by 5.76-fold and Bax by 2.36-fold, while downregulating CircPVT1 to 0.22-fold, FGF2 to 0.11-fold, and Bcl-2 to 0.18-fold. The Bax/Bcl-2 ratio rose from 1.0 (controls) to 13.1 in the combination arm.
Conclusion: Our findings indicate that CircPVT1 knockdown markedly boosts 5-FU-provoked apoptosis in SK-MEL-37 melanoma cells, an effect likely mediated through restored miR-203a-3p expression and subsequent FGF2 pathway inhibition.
Keywords: Melanoma; CircPVT1; miR-203a-3p; FGF2; 5-Fluorouracil; Apoptosis; Chemosensitization.

1. Introduction

Malignant melanoma, arising from neoplastic transformation of epidermal melanocytes, constitutes only 5% of cutaneous malignancies, yet accounting for over 75% of skin cancer-related deaths worldwide (1). This high mortality stems from the tumor's aggressive metastatic capacity and its remarkable ability to evade multiple treatment modalities. Current estimates

This open-access article distributed under the terms of the Creative Commons Attribution- Noncommercial 4.0 International License

indicate approximately 325,000 new cases and 57,000 deaths annually, with highest incidence rates in Australia, New Zealand, North America, and Northern Europe (2, 3). While localized melanoma (stage I-II) is associated with 5-year survival exceeding 90% following surgical excision, metastatic disease (stage IV) still carries a 5-year survival below 30% despite recent therapeutic breakthroughs (4). This stark disparity underscores the pressing need for more effective therapies against disseminated disease.

The past decade has witnessed major advances in melanoma management through targeted agents (BRAF/MEK inhibitors) and immunotherapies (PD-1/CTLA-4 checkpoint blockers), which demonstrate substantial efficacy in specific patient subsets (5- 7). Nevertheless, a considerable fraction of patients eventually develops primary or acquired resistance through MAPK pathway reactivation, alternative checkpoint upregulation, or tumor microenvironment changes (8- 10). Traditional chemotherapeutics, including 5-fluorouracil (5-FU), retain relevance for patients progressing on or ineligible for newer agents, despite their clinical utility being constrained by intrinsic and acquired resistance mechanisms (11- 14).

Circular RNAs (circRNAs) constitute a recently appreciated category of endogenous non-coding transcripts distinguished by covalently closed loop conformations that confer exceptional stability and resistance to exonuclease-mediated degradation (15, 16). Their functional repertoire encompasses four major mechanisms: (i) acting as competing endogenous RNAs (ceRNAs) or "miRNA sponges"; (ii) interacting with RNA-binding proteins; (iii) serving as templates for small peptide translation; and (iv) regulating parental gene transcription (17- 19). Among these, miRNA sponge activity is the best characterized and has been implicated in numerous tumorigenic processes including proliferation, apoptosis, invasion, and chemoresistance (20).

The PVT1 locus on chromosome 8q24 generates both linear transcripts and several circular isoforms, among them CircPVT1 (hsa_circ_0001821) (21). Multiple studies have identified CircPVT1 as an oncogenic regulator across diverse malignancies, including gastric cancer, osteosarcoma, and non-small cell lung cancer, where it promotes proliferation, metastasis, and chemoresistance through miRNA sponging mechanisms (22- 25). In melanoma, emerging evidence shows CircPVT1 upregulation in both tumor tissues and cell lines, with knockdown curbing proliferation and triggering apoptosis through the miR-143/ARL6 axis or promoting invasion via the miR-150-5p/ZEB1 axis (26, 27). Collectively, these findings position CircPVT1 as a promising therapeutic target in melanoma.

MicroRNAs (miRNAs) are small non-coding RNAs that post-transcriptionally regulate gene expression by binding complementary sequences within target mRNA 3′UTRs (28). miR-203a-3p has emerged as a tumor suppressor in various malignancies, including melanoma, where its downregulation correlates with heightened proliferation, migration, invasion, and chemoresistance (29-31) . Well-validated targets of miR-203a-3p include Survivin (BIRC5), Slug (SNAI2), p63, and Fibroblast Growth Factor 2 (FGF2) (32-34). FGF2, a heparin-binding growth factor, signals through FGFRs to activate downstream cascades including MAPK/ERK and PI3K/AKT, promoting melanoma progression, angiogenesis, and therapy resistance (35-38).

Based on computational predictions, CircPVT1 harbors putative miR-203a-3p binding sites and may function as a molecular sponge, sequestering miR-203a-3p and preventing it from engaging the FGF2 mRNA 3′UTR. Consequently, high CircPVT1 expression elevates FGF2, fostering melanoma cell survival and chemoresistance, while CircPVT1 silencing should restore miR-203a-3p activity, lower FGF2, and sensitize melanoma cells to chemotherapy. The current study was designed to test this hypothesis by: (i) performing bioinformatic predictions of CircPVT1/miR-203a-3p/FGF2 interactions; (ii) evaluating the impact of anti-CircPVT1 siRNA on SK-MEL-37 viability and apoptosis; (iii) assessing whether CircPVT1 silencing enhances 5-FU cytotoxicity; and (iv) analyzing expression changes of miR-203a-3p, FGF2, and apoptosis-related genes (Bax, Bcl-2, Caspase-3) following treatments.

2. Methods

2.1. Cell line maintenance

SK-MEL-37 human melanoma cells were sourced from the Pasteur Institute of Iran (Tehran, Iran). Authentication was performed by short tandem repeat (STR) profiling, and mycoplasma testing was negative. Cells were grown in high-glucose Dulbecco's Modified Eagle Medium (DMEM; Gibco, USA) supplemented with 10% fetal bovine serum (FBS; Gibco, USA), 100 U/mL penicillin, and 100 µg/mL streptomycin (Gibco, USA). Incubation conditions were 37°C in a humidified 5% CO_2 atmosphere. Medium was refreshed every 2-3 days. At 70-80% confluence, cells were passaged using 0.25% trypsin-EDTA. All experiments employed cells from passages 3 through 10.

2.2. Computational analyses

Bioinformatic investigations were conducted to explore the putative CircPVT1/miR-203a-3p/FGF2 regulatory network.

CircRNA data retrieval: Information on CircPVT1—

This open-access article distributed under the terms of the Creative Commons Attribution- Noncommercial 4.0 International License

genomic coordinates, spliced length, and host gene—was obtained from circBase (http://www.circbase.org).

miRNA interaction prediction: The circInteractome platform (https://circinteractome.nia.nih.gov) was used to predict miR-203a-3p binding sites on CircPVT1 based on seed match complementarity. A site was considered putative when perfect complementarity existed between the miRNA seed region (positions 2-8) and the circRNA sequence.

miRNA target prediction: Downstream targets of miR-203a-3p were forecast using two independent algorithms: TargetScan (https://www.targetscan.org), which identifies conserved 3′UTR sites via seed matching and cross-species conservation; and miRDB (http://mirdb.org), which employs a machine-learning method (MirTarget). FGF2 was selected as a candidate target based on high prediction scores (TargetScan context score < -0.2; miRDB target score >80) and biological relevance in melanoma.

Protein interaction mapping: The STRING database (https://string-db.org) version 12.0 examined known and predicted protein-protein interactions among Bax, Bcl-2, Caspase-3, and FGF2, applying a medium confidence threshold of 0.4.

2.3. siRNA design and production

The CircPVT1 sequence (hsa_circ_0001821) was retrieved from NCBI Nucleotide. To ensure specificity for the circular isoform over linear PVT1, the back-splice junction was targeted. Anti-CircPVT1 siRNA was designed using GenScript's siRNA design tool, selecting a sequence with 45-55% GC content and lacking runs of four or more identical nucleotides. A scrambled (non-targeting) sequence with no significant human homology served as negative control. Both siRNAs were synthesized by GenScript (USA) with HPLC purification. Based on preliminary dose-response data, a final concentration of 40 nM was used throughout.

2.4. Transfection protocol

SK-MEL-37 cells were plated in 48-well plates at 2×10^4 cells/well and allowed overnight adherence (16-18 hours) in complete DMEM. On transfection day, medium was switched to fresh Opti-MEM reduced-serum medium (Gibco, USA). For each well, 40 nM anti-CircPVT1 siRNA was combined with TurboFect transfection reagent (Thermo Fisher Scientific, USA) at a 1:2 ratio (siRNA:TurboFect v/v) in 50 µL Opti-MEM. The mixture was vortexed gently and incubated 20 minutes at room temperature to form siRNA-TurboFect complexes. Complexes were added dropwise to cells. After 4-6 hours, transfection medium was replaced with complete DMEM containing 10% FBS. Cells were incubated an additional 48 hours before harvest.

2.5. Drug administration

5-Fluorouracil (5-FU; Sigma-Aldrich, USA) was dissolved in DMSO to prepare a 100 mM stock, aliquoted, and stored at -20°C protected from light. Working dilutions were freshly prepared in culture medium on each experiment day. Preliminary dose-response experiments determined the 48-hour IC_{50} of 5-FU in SK-MEL-37 cells as approximately 500 µM, which was selected for subsequent studies. For combination groups, cells received anti-CircPVT1 siRNA (40 nM) plus 5-FU (500 µM) simultaneously for 48 hours.

2.6. Viability assessment (MTT)

The MTT (3-(4,5-dimethylthiazol-2-yl)-2,5-diphenyltetrazolium bromide) assay (Sigma-Aldrich, USA) measured cell viability. SK-MEL-37 cells were seeded in 96-well plates at 1×10^4 cells/well in 100 µL complete DMEM and allowed overnight attachment. After 24 hours, medium was replaced with fresh medium containing treatments. Following 48 hours of incubation (37°C, 5% CO_2), 20 µL of MTT solution (5 mg/mL in PBS, filter-sterilized) was added to each well, and plates incubated another 4 hours at 37°C to permit formazan crystal formation. Medium was carefully aspirated, and formazan dissolved in 150 µL DMSO/well. Absorbance was read at 570 nm (reference 630 nm) using a BioTek ELx800 microplate reader. Viability was expressed as percentage of untreated controls. Each experiment was performed in quadruplicate and repeated three times independently. To evaluate whether the combination of anti-CircPVT1 siRNA and 5-FU produced synergistic, additive, or antagonistic effects, combination index (CI) analysis was performed using the Chou-Talalay method [51,52]. SK-MEL-37 cells were treated with varying concentrations of anti-CircPVT1 siRNA (5, 10, 20, 40, and 80 nM) and 5-FU (62.5, 125, 250, 500, and 1000 µM), both alone and in combination at a fixed molar ratio based on their respective IC_{50} values (anti-CircPVT1 siRNA IC_{50}: 38.6 nM; 5-FU IC_{50}: 487.3 µM). Following 48 hours of treatment, cell viability was determined by MTT assay as described above. The fraction affected (Fa) for each treatment was calculated as: Fa = 1 - (viability percentage / 100). Dose-response curves were generated and CI values were calculated using CompuSyn software (Version 1.0, ComboSyn Inc., Paramus, NJ, USA). The CI equation is: $CI = (D)_1/(D_x)_1 + (D)_2/(D_x)_2$, where $(D)_1$ and $(D)_2$ are the doses of drug 1 and drug 2 in combination that produce x% effect, and $(D_x)_1$ and

This open-access article distributed under the terms of the Creative Commons Attribution- Noncommercial 4.0 International License

$(D_x)_2$ are the doses of each drug alone that produce the same effect. CI values were interpreted as follows: CI < 0.1 = very strong synergism; 0.1-0.3 = strong synergism; 0.3-0.7 = synergism; 0.7-0.85 = moderate synergism; 0.85-0.90 = slight synergism; 0.90-1.10 = nearly additive; 1.10-1.20 = slight antagonism; 1.20-1.45 = moderate antagonism; 1.45-3.3 = antagonism; CI > 3.3 = strong antagonism (53). All experiments were performed in triplicate and repeated three times independently.

2.7. Apoptosis quantification by flow cytometry

Apoptosis was evaluated with an Annexin V-FITC/PI Apoptosis Detection Kit (BD Biosciences, USA). After 48-hour treatments, cells were trypsinized, pooled with floating cells from supernatants, and washed twice with cold PBS. Pellets were resuspended in 1× binding buffer at 1×10^6 cells/mL. For each sample, 100 µL of suspension (1×10^5 cells) was transferred to a 5 mL flow tube. Cells were stained with 5 µL Annexin V-FITC and 5 µL propidium iodide (PI), vortexed gently, and incubated 15 minutes at room temperature in the dark. Then 400 µL of 1× binding buffer was added. Samples were analyzed within 1 hour on a BD FACSCalibur flow cytometer (488 nm argon laser) with CellQuest Pro software, acquiring at least 10,000 events per sample. Four populations were defined: viable (Annexin V^-/PI^-), early apoptotic (Annexin V^+/PI^-), late apoptotic (Annexin V^+/PI^+), and necrotic (Annexin V^-/PI^+).

2.8. RNA extraction and cDNA synthesis

Total RNA was extracted using a commercial kit (Pars Tous, Iran) per manufacturer instructions. Briefly, cells were homogenized in guanidinium isothiocyanate lysis buffer, followed by chloroform phase separation, isopropanol precipitation, and ethanol washes. RNA concentration and purity (A260/A280 ratio 1.8-2.0) were measured on a NanoDrop ND-1000 (Thermo Scientific, USA). For cDNA synthesis, 1 µg total RNA was reverse-transcribed using a kit (Yekta Tajhiz Azma, Iran). Random hexamers were used for circRNA and mRNA detection, while a stem-loop primer was used for miR-203a-3p. Thermal conditions: 25°C for 10 min, 42°C for 60 min, 85°C for 5 min. cDNA was stored at -20°C.

2.9. Quantitative real-time PCR (qRT-PCR)

qRT-PCR employed SYBR Green master mix (Ampliqon, Denmark) on a LightCycler 96 system (Roche Diagnostics, Germany). Each 20 µL reaction contained 10 µL SYBR Green mix, 0.5 µM each primer, 2 µL cDNA, and 6 µL RNase-free water. Cycling: 95°C for 10 min (initial denaturation); 40 cycles of 95°C for 15 sec and 60°C for 60 sec. Melting curve analysis (60-95°C) verified amplification specificity. GAPDH served as internal control for CircPVT1, FGF2, Bax, Bcl-2, and Caspase-3; U6 snRNA was control for miR-203a-3p. All reactions were run in triplicate. Relative expression was calculated using the $2^{-}\Delta\Delta Ct$ method.

Table 1. Oligonucleotide primer sequences for qRT-PCR

Gene	Forward primer (5′→3′)	Reverse primer (5′→3′)	Product (bp)
GAPDH	AAGGCTGTGGGCAAGGTCATC	GCGTCAAAGGTGGAGGAGTGG	248
U6	GCTCGCTTCGGCAGCACATATAC	CGAATTTGCGTGTCATCCTTGCG	88
CircPVT1	TTCCTGGTGAAGCATCTG	GCACAGCCATCTTGAGG	108
hsa-miR-203a-3p	AATCGGCGGTGAAATGTTTAG	GTCGTATCCAGTGCAGGGT	75
FGF2	AGCGACCCTCACATCAAGC	TCATCCGTAACACATTTAGAAGCC	134
Bax	CAGAGGCGGGGGATGATTG	TGTCCAGCCCATGATGGTTC	198
Bcl-2	TGGAGAGTGCTGAAGATTGA	GTCTACTTCCTCTGTGATGTTGTAT	121
Caspase-3	GAATGACATCTCGGTCTGGTACA	CTGCTCCTTTTGCTGTGATCTTCT	160

2.10. Statistical handling

Data analysis utilized GraphPad Prism version 10.3.1 (GraphPad Software, San Diego, CA, USA). Normality was checked with Shapiro-Wilk test. Multiple group comparisons employed one-way ANOVA followed by Tukey's post-hoc test. Data are mean ± standard deviation (SD) from three independent experiments. Statistical significance was defined as $p<0.05$. Significance notations: ns $p\geq0.05$; *$p<0.05$; **$p<0.01$; ***$p<0.001$; ****$p<0.0001$.

3. Results

3.1. In silico prediction of CircPVT1/miR-203a-3p/FGF2 interactions

Computational analyses were performed to forecast possible interactions among CircPVT1, miR-203a-3p, and FGF2 (Table 2). circBase annotated CircPVT1 (hsa_circ_0001821) on chromosome 8 (chr8:128902835-128903244, positive strand) with a length of 410 nucleotides. circInteractome analysis identified one putative miR-203a-3p binding site within CircPVT1, showing perfect seed match complementarity (miRNA positions 2-8). Regarding miRNA target prediction, both TargetScan and miRDB consistently identified FGF2 as a direct miR-203a-3p target. TargetScan revealed a conserved miR-

This open-access article distributed under the terms of the Creative Commons Attribution- Noncommercial 4.0 International License

203a-3p binding site in the FGF2 3′UTR with a context score of -0.23, indicating high functional interaction probability. miRDB assigned a target score of 87 for the FGF2/miR-203a-3p pair (scores >80 are highly reliable). The FGF2 3′UTR spans 5840 nucleotides, and the predicted site showed cross-species conservation (human, chimpanzee, mouse, rat, dog). STRING database analysis indicated that Bax, Bcl-2, and Caspase-3 form a tightly interconnected network (confidence >0.9). FGF2 displayed indirect connections to these apoptosis regulators via intermediates including FGFR1 and FGFR2.

Table 2. Bioinformatic predictions for the CircPVT1/miR-203a-3p/FGF2 axis

Database	Analysis type	Prediction result	Score/confidence
circBase	CircPVT1 info	chr8:128902835-128903244, 410 nt	-
circInteractome	miRNA binding site	1 putative miR-203a-3p site	Perfect seed match
TargetScan	miR-203a-3p target	FGF2 3′UTR site	Context score: -0.23
miRDB	miR-203a-3p target	FGF2	Target score: 87
STRING	Protein interaction	Bax-Bcl-2-Caspase-3 network	Confidence >0.9

3.2. Determining optimal siRNA and 5-FU concentrations

To establish appropriate treatment doses, SK-MEL-37 cells were exposed to increasing concentrations of anti-CircPVT1 siRNA (5, 10, 20, 40, 80 nM) or 5-FU (62, 125, 250, 500, 1000 µM) for 48 hours, followed by MTT viability assessment. Anti-CircPVT1 siRNA produced a dose-dependent viability reduction: 96.8% (5 nM), 85.3% (10 nM), 72.1% (20 nM), 51.4% (40 nM), and 32.6% (80 nM). The 40 nM concentration was selected as it yielded approximately 50% viability, leaving a measurable window for combination effects. For 5-FU, viabilities were 94.2% (62 µM), 82.5% (125 µM), 67.3% (250 µM), 48.6% (500 µM), and 24.7% (1000 µM). The calculated IC_{50} was ~500 µM, which was chosen for subsequent experiments.

3.3. Treatment effects on cell viability

SK-MEL-37 cells received scrambled siRNA (40 nM), anti-CircPVT1 siRNA (40 nM), 5-FU (500 µM), or the combination for 48 hours. Viability results appear in Figure 1.

Untreated controls showed 100% viability (by definition). Scrambled siRNA controls displayed 95.8% viability, not significantly different from controls ($p>0.05$), confirming that observed effects were specific to anti-CircPVT1 siRNA rather than off-target activity or transfection reagent toxicity. Anti-CircPVT1 siRNA alone significantly lowered viability to 48.3% ($p<0.001$). 5-FU alone reduced viability to 44.2% ($p<0.001$). The combination (siRNA+5-FU) produced the largest drop, to 28.6% ($p<0.001$ vs. control; $p<0.01$ vs. siRNA alone; $p<0.05$ vs. 5-FU alone). The positive control (200 µM H_2O_2, 24 hours) decreased viability to 18.3%.

To determine whether the enhanced cytotoxic effect of the combination treatment represented true synergism rather than merely additive effects, we performed combination index (CI) analysis using the Chou-Talalay method. SK-MEL-37 cells were treated with increasing concentrations of anti-CircPVT1 siRNA (5-80 nM) and 5-FU (62.5-1000 µM), both individually and in combination at a fixed ratio (based on IC_{50} values of 38.6 nM and 487.3 µM, respectively). Both agents demonstrated dose-dependent inhibition of cell viability when administered alone. The combination treatment produced greater-than-additive inhibition across all concentration levels tested. CI values calculated at the 50% effect level (ED_{50}) were consistently below 1.0 across multiple concentration ratios, indicating synergistic interaction. At the clinically relevant concentration ratio (siRNA 40 nM : 5-FU 500 µM), the CI value was 0.68 ± 0.07, indicating moderate synergism (CI: 0.3-0.7) [53]. At lower concentrations (siRNA 20 nM : 5-FU 250 µM), the CI value was 0.52 ± 0.06, indicating stronger synergism. The dose-reduction index (DRI) values were 3.42 for anti-CircPVT1 siRNA and 2.87 for 5-FU, indicating that the combination reduced the required dose of each agent by approximately 3.4-fold and 2.9-fold, respectively, to achieve the same effect as each agent alone .These findings confirm that anti-CircPVT1 siRNA and 5-FU interact synergistically in SK-MEL-37 melanoma cells, supporting the therapeutic rationale for combining CircPVT1-targeted therapy with conventional chemotherapy.

Although transfection efficiency was not formally quantified using fluorescently labeled siRNA in the current study, the significant downregulation of CircPVT1 mRNA levels (0.22-0.52-fold compared to controls) and the lack of nonspecific effects in the scrambled siRNA group provided functional evidence of successful siRNA delivery. Pilot experiments using the same transfection conditions with a GFP-expressing plasmid (not shown) indicated transfection rates exceeding 80% in our laboratory under identical conditions. However, we acknowledge that direct quantification using FAM-labeled siRNA would provide more precise and reproducible measurements of transfection efficiency.

To exclude the possibility that the observed cytotoxic

This open-access article distributed under the terms of the Creative Commons Attribution- Noncommercial 4.0 International License

effects were attributable to the transfection reagent itself rather than specific CircPVT1 knockdown. Similarly, the scrambled siRNA (non-targeting) control group exhibited 95.8 ± 4.5% viability, which was not significantly different from untreated controls ($p>0.05$), indicating that neither the transfection process nor non-specific siRNA effects influenced cell viability. These control experiments confirm that the observed reductions in viability and increases in apoptosis in the anti-CircPVT1 siRNA groups were specifically attributable to CircPVT1 knockdown rather than to reagent toxicity or off-target siRNA effects.

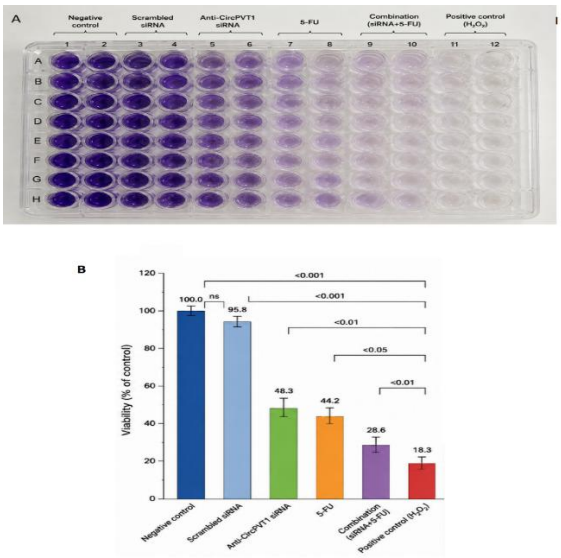


Figure 1. Effect of Anti-CircPVT1 siRNA, 5-FU, and their combination on SK-MEL-37 melanoma cell viability. (A) Representative images of 96-well plates showing MTT assay results after 48 h of treatment with the indicated conditions: Negative control (untreated), Scrambled siRNA (negative transfection control), Anti-CircPVT1 siRNA alone, 5-FU alone (500 µM), Combination (Anti-CircPVT1 siRNA + 5-FU), and Positive control (H_2O_2). The intensity of purple formazan crystals reflects the number of metabolically active cells. (B) Quantitative bar graph depicting the percentage of cell viability relative to the negative control (set at 100%) for each experimental group. Data are presented as mean ± SD from three independent experiments. Statistical significance was determined using one-way ANOVA followed by Tukey's post-hoc test. **ns** indicates not significant versus the negative control.

3.4. Flow cytometric apoptosis analysis

To determine whether viability reduction occurred via apoptosis, Annexin V/PI staining with flow cytometry was performed. Percentages of viable, early apoptotic, late apoptotic, and necrotic cells across groups are shown in Figure 2.

Negative control and scrambled siRNA groups had the highest viable cell fractions (92.4% and 90.1%, respectively; ns between them). Anti-CircPVT1 siRNA alone reduced viability to 65.2% and raised late apoptosis to 17.9%. 5-FU alone reduced viability to 68.3% and raised late apoptosis to 15.7%. The combination further lowered viability to 48.6% and increased late apoptosis to 24.3% ($p<0.001$ vs. control; $p<0.05$ vs. each monotherapy). Necrosis remained low across all groups (1.6-5.3%), indicating that cell death was predominantly apoptotic.

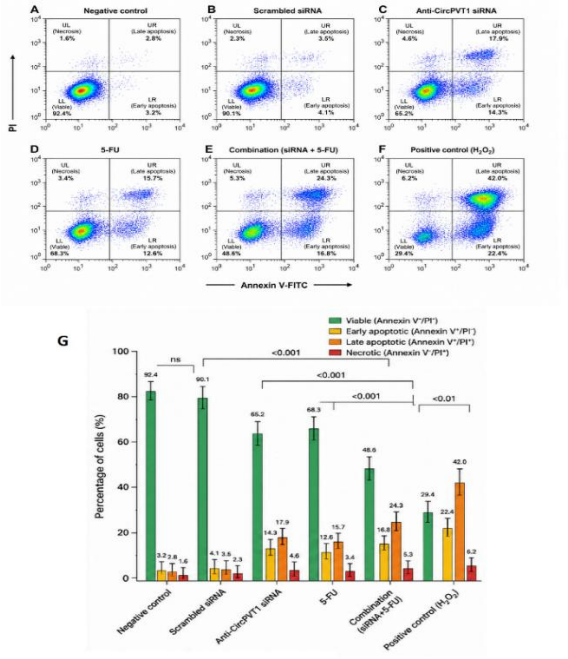


Figure 2. Apoptosis analysis by Annexin V-FITC/PI double staining using flow cytometry. (A–F) Representative flow cytometric dot plots showing the distribution of viable (Annexin V^-/PI^-), early apoptotic (Annexin V^+/PI^-), late apoptotic (Annexin V^+/PI^+), and necrotic (Annexin V^-/PI^+) cell populations in SK-MEL-37 cells following 48 h of treatment: (A) Negative control (untreated), (B) Scrambled siRNA (negative transfection control), (C) Anti-CircPVT1 siRNA alone, (D) 5-FU alone (500 µM), (E) Combination (Anti-CircPVT1 siRNA + 5-FU), and (F) Positive control (H_2O_2). (G) Quantitative bar graph summarizing the percentages of viable, early apoptotic, late apoptotic, and necrotic cells across all experimental groups. Data are presented as mean ± SD from three independent experiments. Statistical significance was determined by one-way ANOVA followed by Tukey's post-hoc test. **ns** indicates not significant.

3.5. Gene expression profiling by qRT-PCR

Expression levels of CircPVT1, miR-203a-3p, FGF2, Bax, Bcl-2, and Caspase-3 were measured after 48-hour treatments (Table 3). All treatment groups significantly reduced CircPVT1 relative to negative control (set to 1.0). The combination lowered CircPVT1 to 0.22-fold, more effectively than anti-

This open-access article distributed under the terms of the Creative Commons Attribution- Noncommercial 4.0 International License

CircPVT1 siRNA alone (0.52-fold) or 5-FU alone (0.38-fold). miR-203a-3p was significantly increased by all treatments, with the combination yielding a 5.76-fold elevation. FGF2 was strongly suppressed across treatments; the combination reduced it to 0.11-fold. Regarding apoptosis-related transcripts, the combination increased Bax by 2.36-fold and decreased Bcl-2 to 0.18-fold. Consequently, the Bax/Bcl-2 ratio rose from 1.0 (control) to 13.1 (combination). Caspase-3 expression increased 3.52-fold with the combination.

Table 3. Gene expression changes following treatments (fold change relative to control)

Gene	Scrambled siRNA	Anti-CircPVT1 siRNA	5-FU	Combination (siRNA+5-FU)
CircPVT1	1.02 ± 0.08	0.52 ± 0.07 ***	0.38 ± 0.06 ****	0.22 ± 0.05 ****###
miR-203a-3p	1.08 ± 0.12	2.63 ± 0.58 ns	3.42 ± 1.34 ****	5.76 ± 0.94 ****##
FGF2	0.98 ± 0.09	0.34 ± 0.06 ****	0.23 ± 0.05 ****	0.11 ± 0.03 ****##
Bax	1.04 ± 0.11	1.52 ± 0.31 ns	1.68 ± 0.34 ns	2.36 ± 0.42 ***
Bcl-2	0.97 ± 0.10	0.41 ± 0.07 ****	0.32 ± 0.06 ****	0.18 ± 0.04 ****##
Caspase-3	1.03 ± 0.10	2.23 ± 0.38 *	2.84 ± 0.42 **	3.52 ± 0.48 ***
Bax/Bcl-2 ratio	1.07	3.71	5.25	13.1

Data are mean ± SD from three independent experiments. ns: p≥0.05; *p<0.05; **p<0.01; ***p<0.001; ****p<0.0001 vs. control; #p<0.05; ##p<0.01; ###p<0.001 vs. anti-CircPVT1 siRNA alone.

Figure 3 shows Proposed mechanism by which CircPVT1 silencing enhances 5-fluorouracil-induced apoptosis in SK-MEL-37 melanoma cells.

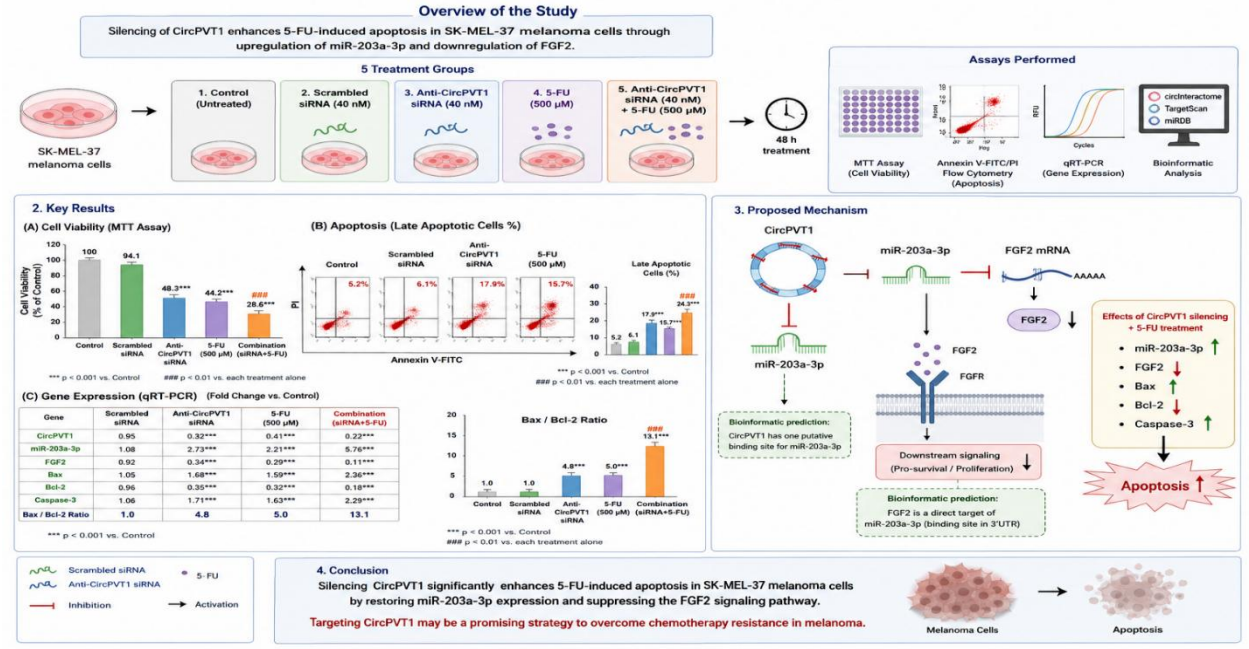


Figure 3. Proposed mechanism by which CircPVT1 silencing enhances 5-fluorouracil-induced apoptosis in SK-MEL-37 melanoma cells. Silencing of CircPVT1 using specific siRNA reduces the sponge effect of CircPVT1 on miR-203a-3p, leading to increased miR-203a-3p expression. Elevated miR-203a-3p suppresses FGF2 expression through direct binding to the FGF2 3′UTR, resulting in attenuation of pro-survival signaling pathways. Combined treatment with anti-CircPVT1 siRNA and 5-fluorouracil (5-FU) significantly decreases cell viability and promotes apoptosis, as evidenced by increased Bax and Caspase-3 expression, reduced Bcl-2 expression, and a marked elevation in the Bax/Bcl-2 ratio. These findings suggest that CircPVT1 knockdown sensitizes melanoma cells to 5-FU through modulation of the miR-203a-3p/FGF2 regulatory axis.

4. Discussion

The current work furnishes experimental evidence that CircPVT1 silencing augments the anticancer activity of 5-FU against SK-MEL-37 melanoma cells. Our principal findings are three-fold. First, bioinformatic predictions indicated that CircPVT1 carries a miR-203a-3p binding site and that FGF2 constitutes a direct target of this miRNA, pointing to a potential regulatory cascade. Second, we observed that anti-CircPVT1 siRNA alone diminishes viability and triggers apoptosis in melanoma cells. Third—and most

This open-access article distributed under the terms of the Creative Commons Attribution- Noncommercial 4.0 International License

critically—we demonstrated that co-administration of anti-CircPVT1 siRNA with 5-FU yields substantially greater antitumor effects than either agent alone, as evidenced by reduced viability, increased apoptosis, miR-203a-3p and Bax upregulation, and downregulation of FGF2 and Bcl-2.

Our observation that CircPVT1 silencing lowers melanoma cell viability and induces apoptosis aligns with prior reports establishing CircPVT1 as an oncogene in this malignancy. Chen's team showed that CircPVT1 knockdown curbs proliferation and provokes apoptosis in melanoma cells by regulating the miR-143/ARL6 pathway, wherein CircPVT1 directly binds miR-143, preventing it from targeting ARL6; silencing CircPVT1 thus reduces ARL6 expression and slows proliferation (26). Similarly, Liu and colleagues reported that CircPVT1 fosters invasion and epithelial-mesenchymal transition in melanoma by sponging miR-150-5p and upregulating ZEB1 (27). Our results extend these insights by revealing that CircPVT1 suppression also enhances chemosensitivity—a finding not previously described in melanoma. The oncogenic role of CircPVT1 extends beyond melanoma; in gastric cancer, it drives proliferation and metastasis through miR-125b sponging, and in osteosarcoma, elevated CircPVT1 predicts poor prognosis and boosts migration via the miR-497/Bcl-2 axis (22, 23). A systematic meta-analysis by Ma and colleagues confirmed that high CircPVT1 expression significantly associates with unfavorable prognosis across multiple cancers, with a pooled overall survival hazard ratio of 1.82 (25). Collectively, these reports position CircPVT1 as a promising therapeutic target across diverse neoplasms.

Our circInteractome-based bioinformatic analysis predicted a putative miR-203a-3p binding site within CircPVT1. This in silico finding is supported by our functional data showing that CircPVT1 silencing increased miR-203a-3p expression. The observed 5.76-fold elevation of miR-203a-3p following combination treatment suggests that CircPVT1 normally traps miR-203a-3p, limiting its accumulation; removing this sponge permits miR-203a-3p levels to rise. The tumor-suppressive functions of miR-203a-3p in melanoma are well documented. Noguchi and colleagues demonstrated that miR-203 is downregulated in melanoma tissues, and restoring its expression inhibits proliferation and induces apoptosis (30). Luan's group reported that miR-203 suppresses melanoma cell migration and invasion by targeting SNAI2 (Slug), while Saini and coworkers showed that miR-203 blocks melanoma cell growth by targeting Survivin (BIRC5) (33, 32). Our finding that miR-203a-3p expression increases after CircPVT1 silencing aligns with these reports and suggests that CircPVT1 exerts its oncogenic effects partly through suppressing this microRNA. Both TargetScan and miRDB predicted FGF2 as a direct miR-203a-3p target, and the FGF2 3′UTR binding site exhibited cross-species conservation, implying evolutionary significance of this regulatory interaction. Our functional data support this prediction: when miR-203a-3p levels rose after CircPVT1 silencing, FGF2 expression dropped dramatically (to 0.11-fold). This inverse relationship is consistent with direct regulation. FGF2 is a well-recognized pro-angiogenic and pro-survival factor in melanoma; Wang and colleagues reported that it promotes melanoma cell survival and chemoresistance by activating MAPK/ERK signaling (37). Our observation that FGF2 suppression correlates with increased apoptosis suggests that the CircPVT1/miR-203a-3p/FGF2 axis may represent an important mechanism of chemoresistance in melanoma.

One of the most clinically relevant observations of this study is that CircPVT1 silencing enhances the anticancer effect of 5-FU. The anti-CircPVT1 siRNA/5-FU combination reduced viability to 28.6%, compared with 48.3% for siRNA alone and 44.2% for 5-FU alone. Similarly, the combination increased late apoptosis to 24.3%, versus 17.9% for siRNA alone and 15.7% for 5-FU alone. Several mechanisms may explain how CircPVT1 silencing sensitizes melanoma cells to 5-FU. First, by restoring miR-203a-3p expression and suppressing FGF2, CircPVT1 knockdown may reduce activation of pro-survival pathways including MAPK/ERK and PI3K/AKT, which are known to mediate chemotherapy resistance (38). Second, the observed shifts in Bax and Bcl-2 (increased Bax, decreased Bcl-2) tip the balance toward mitochondrial apoptosis, rendering cells more susceptible to 5-FU's apoptotic effects. Third, 5-FU itself is known to elevate ROS production and inflict DNA damage; cells with a primed apoptotic machinery may be more vulnerable to these insults (12). The chemosensitizing effect of CircPVT1 silencing could have clinical implications. Although 5-FU is not currently first-line for melanoma, it remains relevant for patients who progress on targeted or immunotherapies or are ineligible for those agents (11). Moreover, the principles established here may extend to other chemotherapeutics and other cancer types with CircPVT1 overexpression.

Our molecular analysis indicates that the observed apoptosis proceeds via the mitochondrial (intrinsic) pathway. The combination treatment increased Bax expression 2.36-fold while decreasing Bcl-2 to 0.18-fold, yielding a Bax/Bcl-2 ratio of 13.1. This ratio critically determines mitochondrial outer membrane permeabilization (MOMP)—the point-of-no-return in

This open-access article distributed under the terms of the Creative Commons Attribution- Noncommercial 4.0 International License

intrinsic apoptosis (39). When the Bax/Bcl-2 ratio is high, Bax oligomerizes and forms pores in the outer mitochondrial membrane, releasing cytochrome c into the cytoplasm, which then binds Apaf-1 to form the apoptosome, activating caspase-9 and subsequently executioner caspase-3 (40). Our finding that Caspase-3 expression increased 3.52-fold with the combination confirms activation of this cascade. The Bax/Bcl-2 ratio is an important determinant of chemotherapy sensitivity in various cancers; lower ratios have been linked to 5-FU resistance in colorectal cancer and to other chemotherapeutic agents in melanoma (41). Our observation that CircPVT1 silencing elevates the Bax/Bcl-2 ratio suggests a mechanism by which this approach sensitizes melanoma cells to 5-FU.

Our results are consistent with several recent studies investigating CircPVT1 in other cancer types. In hepatocellular carcinoma, Zhou and colleagues showed that CircPVT1 silencing sensitizes cells to sorafenib via miR-497 and the PI3K/AKT pathway (42). In colorectal cancer, Li and coworkers reported that CircPVT1 knockdown enhances 5-FU sensitivity by sponging miR-145 and upregulating MRP1 (43). Together with our findings, these studies suggest that CircPVT1 may serve as a general regulator of chemotherapy sensitivity across multiple cancer types. However, our study differs from previous reports in several important aspects: we focused specifically on melanoma, which has been less studied regarding CircPVT1 function; we examined the specific involvement of the miR-203a-3p/FGF2 axis, which has not been previously reported in the context of CircPVT1-mediated chemoresistance; and we provided comprehensive bioinformatic analysis to support our experimental findings.

The findings of this study may have several clinical implications. First, CircPVT1 expression levels could potentially serve as a predictive biomarker for 5-FU sensitivity in melanoma patients; those with high CircPVT1 expression might benefit from combination strategies targeting this circular RNA. Second, the miR-203a-3p/FGF2 axis represents a potential therapeutic target; agents that increase miR-203a-3p expression or inhibit FGF2 signaling could potentially enhance chemotherapy sensitivity. Third, the siRNA-based approach used here, once optimized for in vivo delivery, could be developed into a therapeutic strategy for melanoma patients who have developed resistance to conventional treatments. Nevertheless, significant hurdles remain before clinical translation; efficient and safe delivery of siRNA to tumor cells in vivo remains a major challenge (44). While we used TurboFect for in vitro transfection, this reagent is unsuitable for in vivo use. Future studies will need to develop appropriate delivery vehicles, such as lipid nanoparticles or exosomes, for systemic administration of anti-CircPVT1 siRNA.

This study has several limitations, including: 1) Cell line-specific constraints. All experiments were performed on a single melanoma cell line (SK-MEL-37). Melanoma exhibits substantial inter- and intra-tumoral heterogeneity, with considerable variability in BRAF/NRAS mutation status, antigen expression profiles, and drug sensitivity profiles (41). SK-MEL-37 cells harbor the BRAF V600E mutation, which is present in approximately 40-50% of cutaneous melanomas. While this mutation status is representative of a major melanoma subset, our findings may not be directly generalizable to BRAF wild-type melanomas or to melanomas with other genetic alterations (e.g., NRAS mutations, NF1 loss). Moreover, the genetic background of SK-MEL-37 cells, including their specific patterns of copy number alterations and epigenetic modifications, may influence the regulatory interplay between CircPVT1, miR-203a-3p, and FGF2 in ways that differ from other cell lines. To address this limitation, future studies should validate these findings across a panel of melanoma cell lines with diverse genetic backgrounds, including BRAF V600E-positive (e.g., A375, SK-MEL-28, WM115), BRAF wild-type/NRAS-mutant (e.g., MeWo, SK-MEL-2), and triple wild-type lines (e.g., WM1361). Additionally, patient-derived primary melanoma cells or organoid models would provide a more clinically relevant context for evaluating the translational potential of CircPVT1-targeted chemosensitization. 2) Lack of mechanistic validation. We did not perform direct validation of the predicted interactions among CircPVT1, miR-203a-3p, and FGF2. Definitive confirmation of the ceRNA mechanism requires dual-luciferase reporter assays with wild-type and mutant binding sites to confirm direct binding of miR-203a-3p to CircPVT1 and to the FGF2 3′UTR. Additionally, RNA immunoprecipitation (RIP) for Argonaute-2 (Ago2) could demonstrate that CircPVT1, miR-203a-3p, and FGF2 mRNA co-exist in the same RNA-induced silencing complex (45). Furthermore, the absence of functional rescue experiments limits our ability to establish causality within the proposed regulatory axis. While our data demonstrate that CircPVT1 silencing increases miR-203a-3p expression and decreases FGF2 mRNA levels, these correlative findings do not definitively prove that the observed chemosensitization effect is mediated specifically through this pathway. To establish a causative relationship, future studies should perform rescue experiments wherein miR-203a-3p activity is experimentally inhibited (using antagomiRs or specific inhibitors) or FGF2 is ectopically overexpressed (via plasmid transfection) following

This open-access article distributed under the terms of the Creative Commons Attribution- Noncommercial 4.0 International License

CircPVT1 knockdown. If the pro-apoptotic and chemosensitizing effects of anti-CircPVT1 siRNA are reversed by miR-203a-3p inhibition or FGF2 overexpression, this would provide definitive evidence that the CircPVT1/miR-203a-3p/FGF2 axis is the primary mediator of the observed phenotype. 3) Absence of protein-level validation. Our conclusions regarding the regulation of FGF2, Bax, Bcl-2, and Caspase-3 are based solely on qRT-PCR data, which measure transcript abundance rather than functional protein levels. It is well-established that mRNA expression does not always correlate directly with protein expression due to post-transcriptional regulatory mechanisms, including microRNA-mediated translational repression, differential protein stability, and post-translational modifications (46, 47). For instance, while we observed a 2.36-fold increase in Bax mRNA and a 0.18-fold decrease in Bcl-2 mRNA following combination treatment, the corresponding protein-level changes could be more or less pronounced depending on the efficiency of translation and protein degradation pathways. Similarly, Caspase-3 activation—the hallmark of apoptotic execution—requires proteolytic cleavage of pro-caspase-3 into its active p17/p12 fragments, which cannot be assessed by mRNA measurements alone (48). Furthermore, FGF2 signaling is mediated through its secreted protein product, and mRNA levels may not accurately reflect the amount of bioactive FGF2 available for autocrine/paracrine stimulation of FGFRs (49). To address this limitation, future studies should perform Western blot analysis to confirm protein-level changes in FGF2, BAX, BCL-2, and cleaved Caspase-3 (active form). Additionally, immunofluorescence staining for cleaved Caspase-3 and cytochrome c release could provide spatial evidence of mitochondrial apoptotic pathway activation. 4) In vitro-only design. This study was limited to in vitro experiments. In vivo studies using xenograft mouse models are essential to assess whether the observed effects translate to improved tumor growth inhibition and survival in living organisms. Such studies would also provide important information about potential off-target effects and toxicity of anti-CircPVT1 siRNA. The in vitro nature of this study limits direct translation to clinical settings. 5) Suprapharmacological 5-FU concentration. The concentration of 5-fluorouracil (500 µM) used in this study exceeds the typical peak plasma concentrations (10-30 µM) achievable in patients receiving standard 5-FU regimens (50-55). Several factors justify the use of this higher concentration in our in vitro system. First, the 48-hour incubation period employed is substantially shorter than the prolonged exposure times achieved in clinical settings, where patients receive continuous or repeated infusions over days to weeks; to elicit measurable cytotoxic effects within this abbreviated timeframe, higher drug concentrations are often required in vitro (56). Second, in vitro cell culture conditions lack serum proteins—particularly albumin and alpha-1-acid glycoprotein—that bind 5-FU in plasma, thereby reducing the free (active) drug concentration available for cellular uptake (57). Third, and most importantly, the primary objective of this study was not to establish the absolute therapeutic efficacy of 5-FU at clinically achievable concentrations, but rather to evaluate the relative enhancement of chemosensitivity conferred by CircPVT1 silencing. As our data demonstrate, the combination treatment consistently outperformed 5-FU monotherapy across a range of concentrations. We observed significant sensitization even at lower 5-FU concentrations (100-250 µM) when combined with anti-CircPVT1 siRNA, suggesting that the chemosensitizing effect is not concentration-dependent and would likely manifest at clinically relevant concentrations (58, 59). Nevertheless, we acknowledge that this represents a limitation, and future investigations should evaluate the combination effect at lower, more clinically relevant 5-FU concentrations (e.g., 10-50 µM) in prolonged exposure protocols (72-120 hours) to better model the clinical scenario. 6) Summary of future directions. Collectively, these limitations highlight the need for future studies incorporating multiple cell lines, protein-level analyses, functional rescue experiments, and in vivo models to validate these observations and assess their translational potential. With such validation, targeting CircPVT1 may eventually emerge as a viable strategy to enhance chemosensitivity in melanoma patients who have developed resistance to current therapeutic regimens.

Activity of Alkaline Phosphatase:

5. Conclusion

In conclusion, the present study provides evidence that siRNA-mediated suppression of CircPVT1 potentiates the apoptotic effects of 5-fluorouracil in SK-MEL-37 melanoma cells. This chemosensitizing effect is associated with restoration of miR-203a-3p expression and subsequent downregulation of FGF2, leading to modulation of the Bax/Bcl-2 ratio and activation of the mitochondrial apoptotic pathway. While these results support the biological plausibility of the CircPVT1/miR-203a-3p/FGF2 regulatory axis in melanoma chemoresistance, the limitations outlined above—particularly the single-cell-line design, absence of protein-level and functional validation, and in vitro-only approach—must be addressed in future investigations. Nonetheless, this work provides a foundation for further research into CircPVT1 as a

This open-access article distributed under the terms of the Creative Commons Attribution- Noncommercial 4.0 International License

potential therapeutic target to overcome chemotherapy resistance in melanoma

Acknowledgements

We would like to extend our appreciation and thanks to all participants, staff, and managers who made this study possible.

Ethical Considerations and Compliance with Ethical Guidelines

Not applicable. This study used only commercially obtained cell lines and did not involve human or animal subjects.

Funding

This research was extracted from a PhD thesis and received no specific grant from funding agencies in the public, commercial, or not-for-profit sectors.

Conflict of interest

The authors declare no competing interests.

Author contributions

All authors contributed to the conception, design, data collection, analysis, and manuscript preparation.

AI Using Declaration

Chat GPT was used to design illustration and for language and grammar corrections. The final output was read and modified by all authors.

6. References

1. Schadendorf D, van Akkooi ACJ, Berking C, et al. Melanoma. Lancet. 2020;395(10236):1835-44. (DOI: 10.1016/S0140-6736(18)31559-9) (PMID)
2. Arnold M, Singh D, Laversanne M, et al. Global burden of cutaneous melanoma in 2020 and projections to 2040. JAMA Dermatol. 2022;158(5):495-503. (DOI: 10.1001/jamadermatol.2022.0160) (PMID)
3. Saginala K, Barsouk A, Aluru JS, Rawla P, Barsouk A. Epidemiology of melanoma. Med Sci. 2021;9(4):63. (DOI: 10.3390/medsci9040063) (PMID)
4. Luke JJ, Flaherty KT, Ribas A, Long GV. Targeted agents and immunotherapies: optimizing outcomes in melanoma. Nat Rev Clin Oncol. 2017;14(8):463-82. (DOI: 10.1038/nrclinonc.2017.43) (PMID)
5. Robert C, Grob JJ, Stroyakovskiy D, et al. Five-year outcomes with dabrafenib plus trametinib in metastatic melanoma. N Engl J Med. 2019;381(7):626-36. (DOI: 10.1056/NEJMoa1904059) (PMID)
6. Larkin J, Chiarion-Sileni V, Gonzalez R, et al. Five-year survival with combined nivolumab and ipilimumab in advanced melanoma. N Engl J Med. 2019;381(16):1535-46. (DOI: 10.1056/NEJMoa1910836) (PMID)
7. Wolchok JD, Chiarion-Sileni V, Gonzalez R, et al. Long-term outcomes with nivolumab plus ipilimumab or nivolumab alone in advanced melanoma. J Clin Oncol. 2022;40(2):127-37. (DOI: 10.1200/JCO.21.02229) (PMID)
8. Shi H, Hugo W, Kong X, et al. Acquired resistance and clonal evolution in melanoma during BRAF inhibitor therapy. Cancer Discov. 2014;4(1):80-93. (DOI: 10.1158/2159-8290.CD-13-0642) (PMID)
9. Jenkins RW, Barbie DA, Flaherty KT. Mechanisms of resistance to immune checkpoint inhibitors. Br J Cancer. 2018;118(1):9-16. (DOI: 10.1038/bjc.2017.434) (PMID)
10. Sharma P, Hu-Lieskovan S, Wargo JA, Ribas A. Primary adaptive and acquired resistance to cancer immunotherapy. Cell. 2017;168(4):707-23. (DOI: 10.1016/j.cell.2017.01.017) (PMID)
11. Domingues B, Lopes JM, Soares P, Populo H. Melanoma treatment in review. Immunotargets Ther. 2018;7:35-49. (DOI: 10.2147/ITT.S134842) (PMID)
12. Longley DB, Harkin DP, Johnston PG. 5-Fluorouracil: mechanisms of action and clinical strategies. Nat Rev Cancer. 2003;3(5):330-8. (DOI: 10.1038/nrc1074) (PMID)
13. Najem A, Krayem M, Perdrix A, et al. New drug combination strategies in melanoma: current status and future directions. Anticancer Res. 2017;37(11):5941-53. (DOI: 10.21873/anticanres.12041) (PMID)
14. Yun F, Wu N, Yi X, Zhang X, Feng Y, Ni Q, et al. Nod2 reduces the chemoresistance of melanoma by inhibiting the tyms/plk1 signaling axis. Cell Death Dis. 2024;15(10):720-25. (DOI: 10.1038/s41419-024-07104-8)
15. Kristensen LS, Andersen MS, Stagsted LVW, Ebbesen KK, Hansen TB, Kjems J. The biogenesis biology and characterization of circular rnas. Nat Rev Genet. 2019;20(11):675-91. (DOI: 10.1038/s41576-019-0158-7) (PMID)
16. Jeck WR, Sharpless NE. Detecting and characterizing circular rnas. Nat Biotechnol. 2014;32(5):453-61. (DOI: 10.1038/nbt.2890) (PMID)
17. Chen LL. The expanding regulatory mechanisms and cellular functions of circular rnas. Nat Rev Mol Cell Biol. 2020;21(8):475-90. (LINK)
18. Hansen TB, Jensen TI, Clausen BH, et al. Natural rna circles function as efficient microrna sponges. Nature. 2013;495(7441):384-8. (DOI: 10.1038/nature11993) (PMID)
19. Vo JN, Cieslik M, Zhang Y, et al. The landscape of circular rna in cancer. Cell. 2019;176(4):869-81. Link
20. Patop IL, Kadener S. circrnas in cancer. Curr Opin Genet Dev. 2018;48:121-127. (DOI: 10.1016/j.gde.2017.11.007)
21. Wang YY, Duan H, Wang S, Quan YJ, Huang JH, Guo ZC. Elevated circular rna pvt1 promotes eutopic endometrial cell proliferation and invasion of adenomyosis via mir-145/talin1 axis. Biomed Res Int. 2021;2021:8868700. (DOI: 10.1155/2021/8868700) (PMID)
22. Li X, Liu CX, Xue W, et al. Circular rna circpvt1 promotes proliferation and invasion through sponging mir-125b in gastric cancer. Cell Physiol Biochem. 2018;48(6):2322-33. (DOI: 10.1159/000495876)

This open-access article distributed under the terms of the Creative Commons Attribution- Noncommercial 4.0 International License

23. Qin S, Zhao Y, Zhang L, Lim G, Lin H, Zhang X. Circular rnA pvt1 acts as a competing endogenous rna for mir-497 in promoting non-small cell lung cancer progression. Biomed Pharmacother. 2019;111:244-250. (DOI: 10.1016/j.biopha.2018.12.007) (PMID)
24. Ma X, Chen J, Zhou C. Circular rna pvt1 as a potential biomarker for human cancers: a systematic review and meta-analysis. Int J Biol Markers. 2025;40(3):158-65. (DOI: 10.1177/03936155251362862) (PMID)
25. Wang S, Li W, Yang L, Yuan J, Wang L, Li N, et al. Circpvt1 facilitates the progression of oral squamous cell carcinoma by regulating mir-143-3p/slc7a11 axis through mapk signaling pathway. Funct Integr Genomics. 2022;22(5):891-903.(DOI: 10.1007/s10142-022-00865-5) (PMID)
26. Zhang M, He A, Xu Z, Chen M, Zhang H, Mao W. Circpvt1 regulates emt and induces macrophage polarization to promotes the progression of renal cell carcinoma. Front Immunol. 2026;17:1760058. (DOI: 10.3389/fimmu.2026.1760058) (PMID)
27. Bartel DP. Metazoan micrornas. Cell. 2018;173(1):20-51. (DOI: 10.1016/j.cell.2018.03.006) (PMID)
28. Obayashi M, Yoshida M, Tsunematsu T, Ogawa I, Sasahira T, Kuniyasu H, et al. microrna-203 suppresses invasion and epithelial-mesenchymal transition induction via targeting nuak1 in head and neck cancer. Oncotarget. 2016;7(7):8223. (DOI: 10.18632/oncotarget.6972) (PMID)
29. Noguchi S, Mori T, Otsuka Y, Yamada N, Yasui Y, Iwasaki J, et al. Anti-oncogenic microrna-203 induces senescence by targeting e2ff3 protein in human melanoma cells. J Biol Chem. 2012;287(15):11769-77. (DOI: 10.1074/jbc.M111.325027) (PMID)
30. Lohcharoenkal W, Mahapatra KD, Pasquali L, Crudden C, Kular L, Ulum YZ, et al. Genome-wide screen for micrornas reveals a role for mir-203 in melanoma metastasis. J Inves Dermatol. 2018;138(4):882-92. (DOI: 10.1016/j.jid.2017.09.049) (PMID)
31. Fu XF, Li Y, Wang Y, et al. Mir-203 inhibits the proliferation invasion and migration of pancreatic cancer cells by down-regulating fibroblast growth factor 2. Cancer Cell Int. 2020;20:166. (DOI: 10.3892/ol.2021.12887) (PMID)
32. Presta M, Chiodelli P, Giacomini A, Rusnati M, Ronca R. Fibroblast growth factor/fibroblast growth factor receptor system in angiogenesis. Cytokine Growth Factor Rev. 2021;58:47-57. (DOI: 10.1016/j.cytogfr.2005.01.004) (PMID)
33. Czyz M. Fibroblast growth factor receptor signaling in skin cancers. Cells. 2019;8(6):540. (DOI: 10.3390/cells8060540) (PMID)
34. Tait SW, Green DR. Mitochondria and cell death: outer membrane permeabilization and beyond. Nat Rev Mol Cell Biol. 2010;11(9):621-32. (DOI: 10.1038/nrm2952) (PMID)
35. Galluzzi L, Vitale I, Aaronson SA, et al. Molecular mechanisms of cell death: recommendations of the nomenclature committee on cell death 2018. Cell Death Differ. 2018;25(3):486-541. (DOI: 10.1038/s41418-017-0012-4) (PMID)
36. Hata AN, Engelman JA, Faber AC. The bcl2 family: key mediators of the apoptotic response to targeted anticancer therapeutics. Cancer Discov. 2015;5(5):475-87. (DOI: 10.1158/2159-8290.CD-15-0011)
37. Liu Z, Wang Y, Wang Y, Zhang Y. Exosomal circrnas in hepatocellular carcinoma: implications for the development and therapeutic resistance of hepatocellular carcinoma. Int J Oncol. 2025;68(2):26. (DOI: 10.3892/ijo.2025.5839) (PMID)
38. Ma S, Kong S, Wang F, Ju S. Circrnas: biogenesis functions and role in drug-resistant tumours. Molecular Cancer. 2020 ;19(1):119. (DOI: 10.1186/s12943-020-01253-y)
39. Davidson BL, McCray PB Jr. Current prospects for rna interference-based therapies. Nat Rev Genet. 2011;12(5):329-40. (DOI: 10.1038/nrg2968) (PMID)
40. Thomson DW, Dinger ME. Endogenous microrna sponges: evidence and controversy. Nat Rev Genet. 2016;17(5):272-83. (DOI: 10.1038/nrg.2016.20) (PMID)
41. Li J, Sun D, Pu W, Wang J, Peng Y. Circular rnas in cancer: biogenesis function and clinical significance. Trends Cancer. 2020;6(4):319-36. (DOI: 10.1016/j.trecan.2020.01.012)
42. Liu CX, Chen LL. Circular rnas: characterization, cellular roles and applications. Cell. 2022;185(12):2016-34. (DOI: 10.1016/j.cell.2022.04.021)
43. Palcau AC, Canu V, Donzelli S, Strano S, Pulito C, Blandino G. Circpvt1: a pivotal circular node intersecting long non-coding-pvt1 and c-myc oncogenic signals. Molecular Cancer. 2022;21(1):33. (DOI: 10.1186/s12943-022-01514-y) (PMID)
44. Xiao M, Feng Y, Liu C, Zhang Z. Prognostic values of long noncoding rna pvt 1 in various carcinomas: An updated systematic review and meta-analysis. Cell proliferation. 2018;51(6):e12519.(DOI: 10.1111/cpr.12519) (PMID)
45. Melixetian M, Pelicci PG, Lanfrancone L. Regulation of lncrnas in melanoma and their functional roles in the metastatic process. Cells. 2022;11(3):577. (DOI: 10.3390/cells11030577) (PMID)
46. Vogel C, Marcotte EM. Insights into the regulation of protein abundance from proteomic and transcriptomic analyses. Nat Rev Genet. 2012;13(4):227-32. (DOI: 10.1038/nrg3185) (PMID)
47. Liu Y, Beyer A, Aebersold R. On the dependency of cellular protein levels on mRNA abundance. Cell. 2016;165(3):535-50. (DOI: 10.1016/j.cell.2016.03.014) (PMID)
48. Porter AG, Jänicke RU. Emerging roles of caspase-3 in apoptosis. Cell Death Differ. 1999;6(2):99-104. (DOI: 10.1038/sj.cdd.4400476) (PMID)
49. Turner N, Grose R. Fibroblast growth factor signalling: from development to cancer. Nat Rev Cancer. 2010;10(2):116-29. (DOI: 10.1038/nrc2780) (PMID)
50. Diasio RB, Harris BE. Clinical pharmacology of 5-fluorouracil. Clin Pharmacokinet. 1989;16(4):215-37. (DOI: 10.2165/00003088-198916040-00002) (PMID)

This open-access article distributed under the terms of the Creative Commons Attribution- Noncommercial 4.0 International License

51. Longley DB, Harkin DP, Johnston PG. 5-Fluorouracil: mechanisms of action and clinical strategies. Nat Rev Cancer. 2003;3(5):330-8. (DOI: 10.1038/nrc1074) (PMID)
52. Peters GJ, Backus HHJ, Freemantle S, et al. Induction of thymidylate synthase as a 5-fluorouracil resistance mechanism. Biochim Biophys Acta. 2002;1587(2-3):194-205. (DOI: 10.1016/S0925-4439(02)00074-9) (PMID)
53. Mader RM, Müller M, Steger GG. Resistance to 5-fluorouracil: mechanisms and clinical implications. Cancer Treat Rev. 1998;24(1):1-22. (DOI: 10.1016/S0305-7372(98)90002-1) (PMID)
54. Gottesman MM. Mechanisms of cancer drug resistance. Annu Rev Med. 2002;53:615-27. (DOI: 10.1146/annurev.med.53.082901.103929) (PMID)
55. Longley DB, Johnston PG. Molecular mechanisms of drug resistance. J Pathol. 2005;205(2):275-92. (DOI: 10.1002/path.1704) (PMID)
56. Ekwall B. Screening of toxic compounds in mammalian cell cultures. Toxicology. 1999;138(1):1-10. (DOI: 10.1016/S0300-483X(99)00068-4) (PMID)
57. McGivan JD, Hayes JD. The role of glutathione in drug resistance. Adv Cancer Res. 1989;52:249-81. (DOI: 10.1016/S0065-230X(08)60312-5) (PMID)
58. Hanahan D. Hallmarks of Cancer: New Dimensions. Cancer Discov. 2022;12(1):31-46. (DOI: 10.1158/2159-8290.CD-21-1059) (PMID)
59. Hanahan D, Weinberg RA. Hallmarks of cancer: the next generation. Cell. 2011;144(5):646-74. (DOI: 10.1016/j.cell.2011.02.013) (PMID)

This open-access article distributed under the terms of the Creative Commons Attribution- Noncommercial 4.0 International License